Am J Physiol Cell Physiol 309: C724–C735, 2015.
First published September 2, 2015; doi:10.1152/ajpcell.00182.2015.

CALL FOR PAPERS | *Cell Signaling: Proteins, Pathways and Mechanisms*

A practical method for monitoring FRET-based biosensors in living animals using two-photon microscopy

Wen Tao,[1] Michael Rubart,[2] Jennifer Ryan,[1] Xiao Xiao,[4] Chunping Qiao,[4] Takashi Hato,[1] Michael W. Davidson,[3] Kenneth W. Dunn,[1] and Richard N. Day[5]

[1]*Department of Medicine, Division of Nephrology, Indiana University Medical Center, Indianapolis, Indiana;* [2]*Riley Heart Research Center, Wells Center for Pediatric Research, and Krannert Institute of Cardiology, Indiana University School of Medicine, Indianapolis, Indiana;* [3]*National High Magnetic Field Laboratory and Department of Biological Science, The Florida State University, Tallahassee, Florida;* [4]*Division of Molecular Pharmaceutics, Eshelman School of Pharmacy, University of North Carolina at Chapel Hill, Chapel Hill, North Carolina; and* [5]*Department of Cellular and Integrative Physiology, Indiana University School of Medicine, Indianapolis, Indiana*

Submitted 23 June 2015; accepted in final form 25 August 2015

Tao W, Rubart M, Ryan J, Xiao X, Qiao C, Hato T, Davidson MW, Dunn KW, Day RN. A practical method for monitoring FRET-based biosensors in living animals using two-photon microscopy. *Am J Physiol Cell Physiol* 309: C724–C735, 2015. First published September 2, 2015; doi:10.1152/ajpcell.00182.2015.—The commercial availability of multiphoton microscope systems has nurtured the growth of intravital microscopy as a powerful technique for evaluating cell biology in the relevant context of living animals. In parallel, new fluorescent protein (FP) biosensors have become available that enable studies of the function of a wide range of proteins in living cells. Biosensor probes that exploit Förster resonance energy transfer (FRET) are among the most sensitive indicators of an array of cellular processes. However, differences between one-photon and two-photon excitation (2PE) microscopy are such that measuring FRET by 2PE in the intravital setting remains challenging. Here, we describe an approach that simplifies the use of FRET-based biosensors in intravital 2PE microscopy. Based on a systematic comparison of many different FPs, we identified the monomeric (m) FPs mTurquoise and mVenus as particularly well suited for intravital 2PE FRET studies, enabling the ratiometric measurements from linked FRET probes using a pair of experimental images collected simultaneously. The behavior of the FPs is validated by fluorescence lifetime and sensitized emission measurements of a set of FRET standards. The approach is demonstrated using a modified version of the AKAR protein kinase A biosensor, first in cells in culture, and then in hepatocytes in the liver of living mice. The approach is compatible with the most common 2PE microscope configurations and should be applicable to a variety of different FRET probes.

two-photon excitation; Förster resonance energy transfer; fluorescent proteins; intravital microscopy; biosensor probe; PKA activity

THE IMAGING OF CELLULAR ACTIVITIES within the tissues of live animals using 2-photon excitation (2PE) microscopy has become a powerful tool for determining how cells function in their natural environment (43, 11, 6). Since measurements of cellular activities obtained by intravital microscopy (IVM) are made in the context of intact tissue within the living organism, they can provide a unique perspective on disease processes and the evaluation of therapeutic strategies. The use of exogenous fluorophores, including the fluorescent proteins (FPs), to generate image contrast has greatly enhanced the utility of IVM (25). Of particular interest are the genetically encoded fluorescent reporters, known as biosensor proteins, which allow noninvasive monitoring of the spatial and temporal regulation of cell signaling or metabolic events in situ. The biosensor proteins combine reporter modules containing the FPs with sensing units that are designed to detect specific cell events, such as the activity of kinases, or the binding of small molecules or protein ligands. Many of these biosensor probes rely on Förster resonance energy transfer (FRET) to report the changes in protein conformation or spatial orientation that accompanies the targeted cellular event (5, 19, 37, 39, 40).

These FRET-based biosensor proteins have been exploited extensively in 1-photon excitation (1PE) microscopy but have failed to gain traction in 2PE IVM for several reasons. First, some FPs commonly used in 1PE studies are only weakly excited by 2PE, particularly over the wavelengths provided by the titanium-sapphire lasers used in the vast majority of 2PE microscope systems. Second, many FPs exhibit complex behaviors under multiphoton excitation, and these are often difficult to predict (3, 14, 23). Third, the utility of FRET-based biosensors is confounded by the broad 2PE absorption spectra of FPs (6), which makes it difficult to selectively excite the donor FP of the FRET pair. The resulting spectral cross talk complicates the measurements of FRET by sensitized emission and requires cross talk correction methods specifically developed for 2PE (24). For example, the quantification of FRET from independently produced donor and acceptor probes requires systems equipped with two separate infrared lasers and elaborate cross talk correction methods involving collection of multiple images (24). This problem is partially mitigated when using the linked biosensor probes, since the ratio of the donor to the acceptor is fixed, and the cross talk background is constant.

The use of 2PE creates additional challenges for other methods that are commonly used in 1PE microscopy to determine FRET efficiency. For example, the approach of acceptor photobleaching under 2PE is challenging since it is not possible to selectively excite and bleach only the acceptor FP. The problems of spectral cross talk can be avoided by measuring

Address for reprint requests and other correspondence: R. N. Day, Dept. of Cellular and Integrative Physiology, Indiana University School of Medicine, 635 Barnhill Dr., Indianapolis, IN 46202 (e-mail: rnday@iupui.edu).

the changes in the donor fluorophore lifetime that result from FRET (38), but few investigators have access to a time-resolved 2PE microscopy system. Finally, each of these approaches is time-consuming, requiring extended integration, or collection of multiple images, making them susceptible to motion-induced artifacts in IVM. What is needed for practical 2PE measurements of biosensor activity is a FP pairing with optimal behavior, but with minimal 2PE cross talk. This would allow ratiometric measurements from images collected by IVM using a single 2PE wavelength and also permit a straightforward cross talk correction to determine of the FRET efficiency.

The cyan and yellow FPs have long been favored for FRET-based imaging studies because of their strong spectral overlap. Previous studies characterizing these probes for multiphoton FRET experiments clearly demonstrated that wavelengths near 800 nm were best for selective excitation of CFP over YFP (43). The early versions of the enhanced cyan and yellow FPs (ECFP and EYFP), however, had a number of deficiencies that limited their use for quantitative live-cell imaging approaches (31). Efforts to improve the photophysical characteristics of ECFP by directed mutagenesis yielded a brighter variant called mCerulean (28). Similar approaches were also used to address the deficiencies of EYFP, yielding mVenus (20) and mCitrine (9). Studies of the 2PE characteristics of mCerulean and mVenus showed that excitation at 820 nm reduced the cross talk excitation of mVenus (29). However, mCerulean still has problems associated with photostability (32) and photo-switching behavior (32, 17). To address these shortcomings, mutagenesis was used to substitute residues that influence the planarity of the chromophore, yielding new cyan FPs called mCerulean3 (17) and mTurquoise (7). These cyan FPs are brighter and more photostable than mCerulean and have single-component fluorescence lifetimes (4). These newer generation cyan and yellow FPs share the spectral overlap required for efficient energy transfer, and the improved photophysical characteristics make them most useful for the measurement of FRET.

Here, we systematically evaluate and characterize a number of different FPs for their 2PE characteristics and their suitability when paired for FRET-based biosensor probe applications. Our studies demonstrate that the optimized monomeric (m) Turquoise (7), and mVenus (20) share regions of minimal overlap in their 2PE spectra, making them suitable candidates for 2PE FRET probes. To validate the use of these probes for IVM, a series of linked FRET standards were developed and the FRET measurements by 2PE were confirmed by fluorescence lifetime and acceptor photobleaching methods. These studies demonstrated that FRET probes based on mTurquoise and mVenus enable a simple and robust method for measuring FRET activities in living animals, based on ratiometric measurements obtained from a two-channel 2PE image collected with a single excitation wavelength. We demonstrate that this approach allows the noninvasive and spatiotemporal detection of FRET-based biosensor activities in intact mice using a standard multiphoton microscope system.[1]

[1] This article is the topic of an Editorial Focus by Randall Lindquist and Raluca Niesner (15a).

MATERIALS AND METHODS

Plasmid DNAs and viral vectors. The cDNA sequences encoding the mT-Sapphire, mCerulean, mCerulean3, mTurquoise, mTurquoise2, mTFP1, mVenus, mNeonGreen, Clover, mKO2, and mRuby2 proteins are in the Clontech C1 or N1 plasmid vectors. When expressed individually, the N1 versions with the termination codon at the immediate end of the FP were used. The plasmids encoding the mCerulean-mVenus FRET standards were obtained from Dr. Steven Vogel (National Institutes of Health, Bethesda, MD) and are available from Addgene (Cambridge, MA). Dr. Jin Zhang (Johns Hopkins University) provided the A-kinase activity reporter 4 (AKAR4) plasmid. Recombinant DNA methods were used to replace the sequence encoding mCerulean with that for mTurquoise in the FRET standards and in AKAR4. All plasmid inserts were confirmed by direct sequencing.

The adenovirus (Ad) CMV-Turq-AKAR4 vector was made using the AdEasy system (16). Briefly, sequence encoding Turq-AKAR4 gene was inserted into the pShuttle-CMV vector, which contains some portions of Ad DNA. The resulting pShuttle-CMV-Turq-AKAR4 vector was linearized with *Pme*I and recombined with AdEasy1 in BJ5183 bacterial cells via homologous recombination. The recombinant Ad DNA harboring Turq-AKAR4 gene was digested with *Pac*I to expose inverted terminal repeats of Ad, and then propagated in human embryonic kidney (HEK)293 cells for generation of Ad-CMV-Turq-AKAR4 vector. The Ad-CMV-Turq-AKAR4 vector was purified by two rounds of CsCl density centrifugation, dialyzed, and stored at −70°C in PBS buffer containing 10% glycerol. The virus titer (1.28×10^{12} particles/ml) was determined by measurement of optical density at 260 nm and by counting the fluorescence-positive cells post infection (1×10^{11} infectious U/ml).

Cell culture and transfections. HEK293 cells were maintained in monolayer culture and harvested at 80% confluence. The cells were transfected either using X-tremeGene HP DNA transfection reagent (Roche Diagnostics) or by electroporation. Mouse fetal cardiomyocytes were isolated from hearts harvested from *day 15* embryos by enzymatic digestion with 0.2% collagenase type II in PBS. The enzymatic digestion was stopped after 75 min by diluting the cell suspension with culture medium (DMEM supplemented with 10% FBS, 5 mM Na-pyruvate, 50 μg/ml streptomycin and 50 U/ml penicillin). The cells were maintained in four-well Lab-Tek II chambered coverglass (1.5 borosilicate glass; Thermo Fisher Scientific, Waltham, MA) and incubated in 5% CO_2-95% O_2 at 37°C.

Two-photon microscopy. Nearly all microscopy studies were conducted using an Olympus FV1000 inverted IX 81 spectral type laser scanning confocal microscope modified for two-photon excitation with the addition of a MaiTai Ti-sapphire laser (Spectra-Physics, Santa Clara, CA), a Pockels cell electro-optical attenuator (Conoptics, Danbury, CT), a Keplerian collimator/beam expander, and three gallium arsenide phosphide detectors (Hamamatsu, Middlesex, NJ). Some of the spectral scanning studies (Fig. 1) were conducted using an Olympus FV1000 MPE inverted IX 81 spectral type laser scanning confocal/multiphoton microscope system equipped with a MaiTai DeepSee Ti-sapphire laser (Spectra-Physics). Fluorescence was collected via descanned detectors, using emission filters optimized for each fluorescent protein. Purified FPs (in PBS plus 0.1% BSA solution) or transfected cells (in DMEM-F12 without phenol red) were imaged in Lab-Tek II 2-well chambered coverglasses using an Olympus ×60, 1.2 numerical aperture (NA) water immersion objective. The 2PE fluorescence excitation spectra were obtained by measuring fluorescence emissions over a range of excitation wavelengths using a constant detector gain. The laser power was measured at the specimen plane for each excitation wavelength using a PM100D power meter with λ correction (Thorlabs, Newton, NJ), and adjusted to a constant value.

Intravital microscopy. IVM was conducted as previously described (30) using the modified Olympus FV1000 system described above

with a ×25, NA 1.05 XLPN water immersion objective. Studies were conducted using 11- to 12-wk-old C57BL/6 mice, obtained from Jackson Laboratories (Bar Harbor, ME). In vivo expression of AKAR4.1 was accomplished by viral transduction, via tail vein injection of the Ad-CMV-Turq-AKAR4 vector (4.8×10^{10} viral particles in 200 μl saline per mouse). Seven days after adenovirus injection, mice were fasted for 3 h, anesthetized with isoflurane, and surgically prepared for intravital microscopy. A 2-cm ventral incision was placed just 1 cm below the rib cage to expose the liver, and a small section of PE50 tubing was secured in the abdominal cavity for intraperitoneal injection of glucagon on the stage of the microscope. The left lateral lobe of the liver was carefully lifted and secured to a glass-bottom plate. The mouse was then placed ventral side down on a heated microscope stage and covered with a warming blanket. After identifying an appropriate field of fluorescent cells, a series of image volumes (10 focal planes spaced 1 μm apart) were collected continuously just before and for 15 min following the intraperitoneal injection of 200 μg/kg glucagon, using a heated Olympus ×20, NA 0.95 objective. All studies were approved by the Institutional Animal Care and Use Committee of Indiana University School of Medicine and conformed to the *Guide for the Care and Use of Laboratory Animals* published by the National Institutes of Health (NIH Publication No. 85-23, Revised 1996).

Digital image analysis. Quantitative image analysis was carried out using MetaMorph image processing software (Molecular Devices, Sunnyvale, CA). The relative 2-photon excitation spectra were constructed from the average fluorescence intensity values at the various wavelengths for the purified FPs or for the selected regions of interest (ROI) within the imaged cells. To quantify the average fluorescence intensity, the images collected in *channel 1* and *channel 2* were assembled to separate stacks in MetaMorph. The image planes in a given stack were aligned, and background fluorescence of each plane was measured in a random field outside of cells and subtracted from the corresponding plan for all plans. Then, ROIs with relatively uniform fluorescence within a given cell were selected, and the average fluorescence intensity within these regions was quantified. The same regions were used for both *channel 1* and *channel 2*. The normalized average fluorescence intensity values were calculated for each selected region and then pooled and averaged with those derived from other cells. All the FRET quantifications including FRET efficiency (E_{FRET}) calculations are based on background-subtracted images without any further processing.

Here, the cells expressing the individual FPs or the FRET standards are used to characterize 2PE spectral cross talk components for the donor (mTurquoise) and acceptor (Venus) excitation at 810 nm. The B and A correction factors for the Turquoise emission cross talk and the Venus direct excitation cross talk, respectively, allow the determination of the corrected FRET signal (2).

$$\mathrm{FRET_{corr}} = \mathrm{FRET_{raw}} - \mathrm{ASBT} - \mathrm{DSBT} \quad (1)$$

which is related to the intensity (I) signal as:

$$\mathrm{FRET_{corr}} = I_{FRET} - A * I_{FRET} - B * I_{Turq} \quad (2)$$

Using 810 nm 2PE of cells expressing mTurquoise alone allowed determination of the B correction factor (0.295 ± 0.002). Similarly, cells expressing only mVenus were measured at both 810 nm and 960 nm, and acceptor cross talk component was determined to be 0.030 ± 0.001. Next, the FRET standards (Fig. 2), as well as cells expressing a mixture of mTurquoise and mVenus, were used to determine the average $I_{Ven\text{-}810}/I_{Ven\text{-}960}$ of 0.344 ± 0.046. From this, the correction for acceptor intensity at 810 nm was determined to be 2.91 ± 0.39. Thus, the correction factor A is 2.91 × 0.03 = 0.087 ± 0.01 and the $\mathrm{FRET_{corr}}$ can be defined as:

$$\mathrm{FRET_{corr}} = I_{FRET} - 0.087 * I_{FRET} - 0.295 * I_{Turq} \quad (3)$$

Visualization of FRET signals in images, subsequent processing, FRET image analysis, and generation of ratio images of FRET/Turquoise were performed as described by Broussard (2). The corrected FRET signal is determined using *Eq. 3* in RESULTS. The ratio image of FRET/Turquoise is calculated from the equation:

$$\mathrm{FRET/Turquoise} = \left[\mathrm{FRET_{corr}} * 1,000/I_{\max(\mathrm{FRET_{corr}})}/I_{T\text{-}810} * 1,000/I_{\max(T\text{-}810)}\right] * 100 \quad (4)$$

Both the numerator ($\mathrm{FRET_{corr}}$) and denominator ($I_{T\text{-}810}$) are normalized to the corresponding maximum gray values (I_{max}). Since the pixel values of nonfloating point images are integers, the factor of 100 is included in the resultant ratio images to avoid fractional pixel values in 8-bit images for visualization.

The 2PE FRET efficiency is calculated as previously described (24, 26, 2) using the equation:

$$E = D_{lost}/D_{total} = D_{lost}/\left(D_{lost} + D_{remains}\right) \quad (5)$$

where

$$\mathrm{D_{lost}} = \mathrm{FRET_{corr}} * \left(QY_d/QY_a\right) * \left(S_d/S_a\right) * \left(G_d/G_a\right), \quad \text{and} \quad D_{remains} = I_{Turq\text{-}810} \quad (6)$$

QY_d and QY_a denote the quantum yields of the donor and acceptor, respectively, where the quantum yield ratio for Turquoise and Venus is 1.474 (7, 20). S_d and S_a denote the spectral sensitivities of the donor and acceptor channels. The S_d/S_a ratio is approximated by the bandwidth ratio of *channel 1* and *channel 2*, which is set to 2/3. G_d and G_a are the detector gains for the donor and acceptor emission channel.

FLIM measurements. The fluorescence lifetime measurements are made using the ISS Alba FastFLIM system (ISS, Champagne, IL) coupled to an Olympus IX71 microscope equipped with a ×60, 1.2 NA water immersion objective lens. A Pathology Devices (Pathology Devices) stage top environmental control system maintains the temperature at 36°C and CO_2 at 5%. For FD FLIM using the cyan and yellow FPs the 5 mW 440 nm diode laser is modulated by the Alba FastFLIM system at a fundamental frequency of 10 MHz, with additional measurements at 13 sinusoidal harmonics (10–140 MHz). The modulated laser is coupled to the confocal scanning system, which is controlled by the VistaVision software (ISS). The fluorescence signals emitted from the specimen are routed by a 495 nm long pass beam splitter through the 530/43 nm (acceptor emission) and 480/40 (donor emission) band-pass emission filters, and the signals are detected using two identical avalanche photodiodes. The phase delays and modulation ratios of the emission relative to the excitation are measured at each pixel of an image for each frequency. The most accurate lifetime determinations are obtained by analyzing the first 12 frequencies (10–120 MHz), with the quality of the fit judged by the reduced χ^2 values for the multifrequency response curves (4). The ratio of the donor lifetimes determined in the absence (τ_D) and in the presence of the acceptor (τ_{DA}) provides a direct estimate of FRET efficiency (E_{FRET}) by:

$$E_{FRET} = \left(1 - \tau_{DA}/\tau_D\right) \quad (7)$$

RESULTS

Identification of optimal FPs for 2PE biosensor probes. To identify FPs with properties that are optimal for 2PE IVM measurement of FRET-based biosensor activities, we characterized a series of blue to green FPs as potential donor fluorophores for these probes (Fig. 1*A*). Although the titanium sapphire lasers used in most current 2PE microscope systems are capable of providing emissions over a range of approximately 700 nm to 1,050 nm, optimal power is found in the range between 800 and 900 nm. Accordingly, we focused on donor fluorophores with 2PE in this range. Acceptor fluoro-

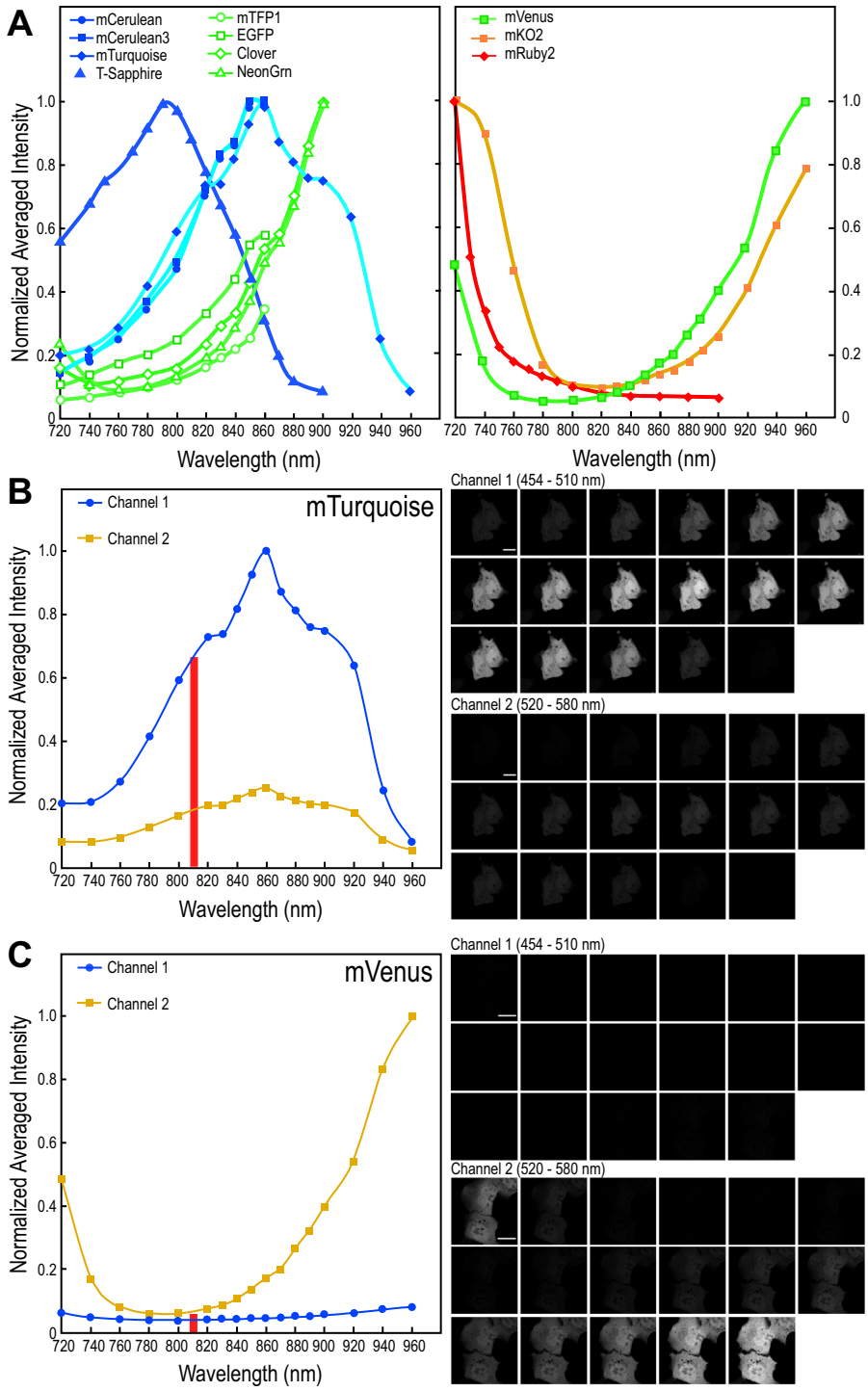

Fig. 1. *A*: two-photon excitation (2PE) spectral scanning of the indicated fluorescent proteins (FPs) expressed individually in living cells. *B* and *C*: the relative 2PE spectral scans for monomeric (m) Turquoise (*B*) and mVenus (*C*), each expressed individually in living cells. The emission signals at the different excitation wavelengths were simultaneously detected in *channel 1* (cyan, 454–510 nm) and *channel 2* (yellow, 520–580 nm), and the images were acquired at each wavelength step (scale bar, 10 μm). Red bar indicates excitation at 810 nm.

phores were identified based on 1P spectral overlap with donor fluorophores and the absence of untoward effects of excitation at wavelengths near 800 nm. For example, some FPs showed a discrete band of very strong emission with illumination near 720 nm, which corresponds to excitation into higher energy electronic levels (6) (see Fig. 1*A*) and results in rapid and irreversible photobleaching at these wavelengths (our unpublished observations).

These criteria narrowed the potential group of donor and acceptor FPs suitable for the IVM approach described here to the newer cyan and yellow FPs, and some of the long stokes shift FPs. Since many existing FRET-based biosensor probes were developed with earlier variants of the cyan and yellow FPs, most imaging systems are set up for the detection of these probes, offering additional advantages to investigators who wish to utilize them for IVM. Spectral scanning showed that the spectral characteristics for each of the cyan variants were similar (Fig. 1*A*), with peak excitation at 860 nm falling to minimal excitation at 960 nm, and there was no enhanced excitation at wavelengths below 780 nm. The improved quan-

tum yield and photostability of mCerulean3 (17), mTurquoise (7), and mTurquoise2 (8) make them attractive donor fluorophores for the development of new biosensor probes, especially when paired with well-characterized acceptors, such as Venus (20) or Citrine (9).

The relative 2PE spectra of mTurquoise and mVenus are shown in Fig. 1, *B* and *C*. The emission signals at the different excitation wavelengths were simultaneously detected in *channel 1* (cyan, 454–510 nm) and *channel 2* (yellow, 520–580 nm) to allow efficient determination of spectral bleed under conditions where there is no FRET. The comparison of the relative 2PE spectra for mTurquoise and mVenus, determined from either the purified proteins in solution, or from each protein expressed independently in living cells, demonstrates a clear nadir in the 2PE for mVenus between 800 nm and 820 nm (~3% of its 960 nm maxima), while these wavelengths are near the peak 2PE of mTurquoise (Fig. 1, *B* and *C*). Thus, when mTurquoise and mVenus are used as FRET pair, the combination of their 2PE spectral characteristics permit efficient excitation of the donor using wavelengths within the 800–820 nm range, while minimizing the direct excitation of the acceptor, as previously observed for other cyan and yellow FP variants (29, 43). Our subsequent studies with biosensor probes using mTurquoise and mVenus exploit this selective excitation at 810 nm.

Characterization of 2PE FRET measurements. To validate mTurquoise and mVenus as fluorophores for FRET-based measurements using IVM, we adopted the "FRET standard" approach (13, 34). For the FRET standards, and subsequent biosensor measurements, the emission signals at the different excitation wavelengths were simultaneously detected in *channel 1* (cyan, 454–494 nm) and *channel 2* (yellow, 520–580 nm), or a bandwidth ratio of 2/3. Fusion proteins with high FRET efficiency were generated by coupling mTurquoise to mVenus through short peptide linkers of 5 or 10 amino acids (AA; see Fig. 2*A*). In contrast, a fusion protein with low FRET efficiency was generated by linking mTurquoise to mVenus through the 229-AA tumor necrosis factor receptor-associated factor 2 (TRAF2) domain (22, 34). In addition, as a control for environmental effects on the donor FP, another fusion protein was generated using a mutant variant of mVenus called Amber. Amber is a nonfluorescent form of mVenus, where the chromophore tyrosine is converted to a cysteine (Y67C), producing a protein that folds correctly, but does not act as a FRET acceptor (13).

In principle, since biosensor probe measurements are of intramolecular FRET between a donor and an acceptor that are always at a 1:1 ratio, it is not necessary to correct for spectral cross talk. However, because the 2PE cross talk components can be substantial, removing the cross talk signals from the FRET measurement will improve the sensitivity and reproducibility of the measurements (2, 26). An additional constraint for our IVM approach is that current technology makes it impractical to rapidly switch and calibrate 2PE wavelengths for each time point. Therefore, we developed an approach for spectral cross talk correction of biosensor probe measurements that uses a single 2PE wavelength.

The spectral bleedthrough (SBT) components that contaminate the FRET signal result from the donor (mTurquoise) emission that bleeds into the acceptor detection channel (DSBT), and from the direct excitation of the acceptor (mVenus) at the donor excitation wavelength (ASBT). The corrected FRET signal ($FRET_{corr}$) is determined by subtracting the cross talk components from the raw FRET signal (donor excitation, acceptor emission). The correction factors A and B that define the direct excitation of Venus (acceptor) and the Turquoise (donor) emission cross talk into the FRET channel are determined from measurements of cells that express each FP alone, and are specific to the microscope system (see MATERIALS AND METHODS).

Measurements of the FRET standards using 2PE. Here, control cells expressing either a mixture of mTurquoise and mVenus or the mTurquoise-based FRET standards (Fig. 2) are used to verify FRET measurements by sensitized emission. The results are then corroborated using both fluorescence lifetime imaging microscopy (FLIM) and acceptor photobleaching measurements (Table 1). The 2PE spectral characteristics of FRET standards were determined using 2PE at 810 nm (Fig. 2*B*). As expected, the sensitized emission measurements demonstrated that there was very little energy transfer between the unlinked FPs, and this was confirmed by both the FLIM and acceptor photobleaching measurements (Table 1). The 2PE measurements for cells expressing low FRET efficiency standard mTurquoise-TRAF-mVenus revealed 2PE spectral profiles similar to those of the unlinked mTurquoise and mVenus mixture (Fig. 2*B*, compare *top right* and *bottom right*). The 2PE ratiometric method demonstrated a low E_{FRET} of 5.2% for mTurquoise-TRAF-mVenus, which was again comparable to that made by the FLIM measurements (Table 1). In contrast, measurements from the cells expressing the high efficiency FRET standard, mTurquoise-5AA-Venus, showed significant quenching of the donor signal (*channel 1*, Fig. 2*B*) with concomitant increase in sensitized acceptor emission (*channel 2*). The FRET measurements using 2PE at 810 nm demonstrated a FRET efficiency (E_{FRET}) of 47.3%, and a similar E_{FRET} was determined with FLIM and verified by acceptor photobleaching (Table 1).

To demonstrate the sensitivity of the 2PE ratiometric approach, a second FRET standard with a longer linker, mTurquoise-10AA-Venus, was also measured. The 2PE ratiometric method demonstrated that increasing the linker length by 5AA resulted in an E_{FRET} of 36.2%, a decrease of 11.1%, compared with the FRET standard with the shorter linker (Table 1). Again, these results were verified by the FLIM measurements (Table 1). Representative FRET ratio images obtained from cells expressing the different FRET standard fusion proteins are shown in Fig. 2*C*. Together, these results demonstrate a simple and robust 2PE ratiometric method that can be used to obtain accurate measurements of E_{FRET} with high sensitivity from the linked probes expressed in living cells.

Measurements of the FRET-based biosensor probe activities using 2PE. To demonstrate that the 2PE ratiometric method can be applied to the measurements of cellular activity with a biosensor probe, we next examined the activity of the protein kinase A (PKA) pathway using the well-characterized A-kinase activity reporter (AKAR) (39, 42). The latest iteration of the AKAR probe, AKAR4, consists of Cerulean coupled to a circular permuted Venus through a linker containing the low-affinity phosphorylated substrate binding domain, FHA1, and the PKA-specific substrate sequence (LRRA*TLVD). The AKAR4 probe has increased the dynamic range compared with earlier variants (42). Since mTurquoise has the desired 2PE

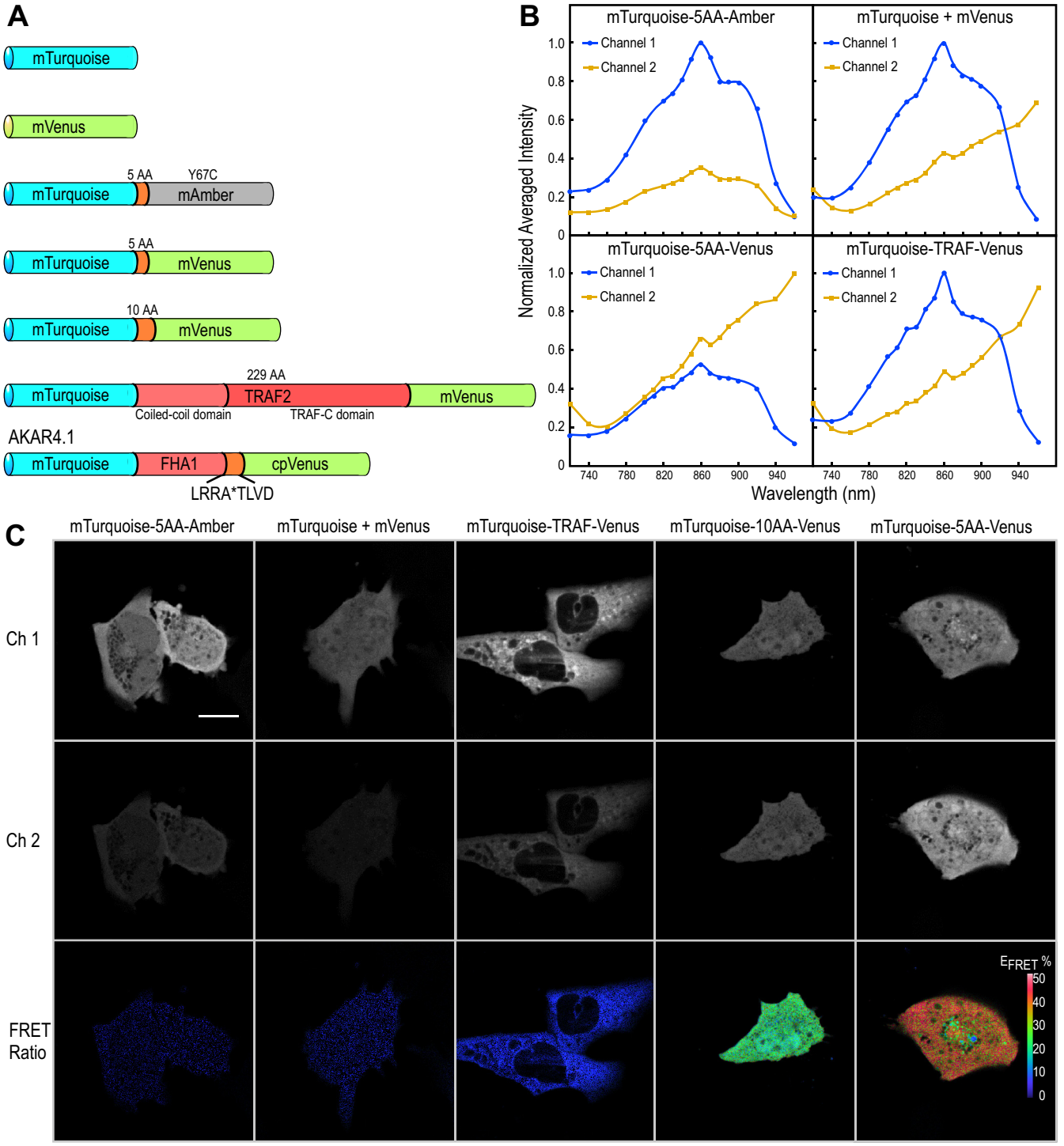

Fig. 2. *A*: schematic representation of the Förster resonance energy transfer (FRET) standard probes and the A-kinase activity reporter (AKAR) 4.1 probe used in this study. *B*: the relative 2PE spectral scans obtained from cells expressing the indicated FRET standard probes excited by illumination at 810 nm. *C*: representative donor intensity [channel (Ch) 1, 454–494 nm; scale bar, 10 μm], acceptor intensity (Ch 2, 520–580 nm), and FRET ratio images obtained from cells expressing the indicated FRET standard probes.

characteristics, improved brightness and photostability, and a single-component lifetime, we replaced the Cerulean FP in AKAR4 with mTurquoise (AKAR4.1; Fig. 2*A*).

HEK293 cells expressing the AKAR4.1 reporter were illuminated at 810 nm, and the emission signals were simultaneously monitored in the cyan (454–494 nm) and yellow (520–580 nm) channels. The baseline emission signals were determined, and forskolin (Fsk) was then added to a final concentration of 24 μM (Fig. 3). Upon addition of Fsk, there was an increase in the emission detected in the Venus channel, with a concomitant decrease in the signal detected in the cyan channel over a 2.5-min time frame, yielding a 1.4-fold change

Table 1. *Comparison of FRET efficiencies determined by 2PE radiometric method and FLIM for different FRET standards*

	2PE Ratiometric	Lifetime				
FRET Standard[a]	E_{FRET}[b] (% ± SD)	2-Component Lifetime (Fraction)	Tau(f)[c] ± SD	Tau(α)[d] ± SD	E_{FRET}[e] (% ± SD)	Acceptor Photobleach
Cerulean-5AA-Amber	ND	2.2 ns (0.66) 4.6 ns (0.34)	3.0 ± 0.05	NA	0	ND
Cerulean-5AA-Venus	ND	3.0 ns (0.55) 1.2 ns (0.45)	NA	1.8 ± 0.07	41.1 ± 2.4	ND
Turquoise + Venus mix	2.0 ± 1.1	3.9 ns (0.99)	3.9 ± 0.07	NA	0	Pre: 3.9 ± 0.07 Post: 3.9 ± 0.04
Turquoise-5AA-Amber	−1.9 ± 0.9	3.8 ns (0.99)	3.8 ± 0.04	NA	0	NA
Turquoise-5AA-Venus	47.3 ± 6.1	3.3 ns (0.69) 1.3 ns (0.31)	NA	2.3 ± 0.08	40.8 ± 1.8	Pre: 2.2 ± 0.05 Post: 3.8 ± 0.04
Turquoise-10AA-Venus	36.2 ± 4.0	3.3 ns (0.74) 1.6 ns (0.27)	NA	2.4 ± 0.07	36.5 ± 2.4	Pre: 2.4 ± 0.04 Post: 3.7 ± 0.03
Turquoise-TRAF-Venus	5.0 ± 3.6	3.6 ns (0.99)	3.6 ± 0.04	NA	7.3 ± 1.0	Pre: 3.6 ± 0.04 Post: 3.7 ± 0.03

[a]Produced in cells at 37°, $n = 3$ or more cells. [b]Determined by the formula devised in this study (see RESULTS and MATERIALS AND METHODS). [c]Tau(f) is the average lifetime. [d]Tau(α) is the amplitude-weighted lifetime. [e]Determined by: $E_{FRET} = (1 - \tau_{DA}/\tau_D)$. FRET, Förster resonance energy transfer; 2PE, two-photon excitation; E_{FRET}, FRET efficiency; TRAF, TNF receptor-associated factor; ND, not detected; NA, not applicable.

in emission ratio of Ven/Turq ($n = 11$ cells). Significantly, the change in the Ven/Turq ratio is only observed in the cytosolic compartment, with no change in the AKAR signal from the nuclear compartment (Fig. 3*B*). This is consistent with the slow translocation of the catalytic subunit of PKA into the nucleus after its dissociation from the regulatory subunits in the cytoplasm upon cAMP elevation (21). These results were confirmed and extended using frequency domain FLIM measurements of the AKAR4.1 probe activity. Lifetime measurements, acquired prior to addition of Fsk, demonstrated that, under basal conditions, the probe population adopts conformations that result in an average E_{FRET} of 38%. Upon addition of Fsk there was a rapid decrease in the mTurquoise lifetime, corresponding to a 12% increase in E_{FRET} (Fig. 3*C*). The changing cytosolic, but not nuclear, PKA activity, is demonstrated by the ratio imaging (Fig. 3*B*) and the fluorescence lifetime maps (Fig. 3*D*).

To demonstrate that the 2PE ratiometric method can be applied to more physiologically relevant models, the intracellular PKA activities in response to Fsk were measured using the AKAR4.1 biosensor in isolated primary mouse fetal cardiomyocytes. Freshly isolated primary cardiomyocytes were transfected with plasmids encoding either the AKAR4.1 or the mTurquoise-10AA-Venus FRET standard (Fig. 4). The 2PE FRET imaging demonstrated that the addition of Fsk to cells expressing AKAR4.1 resulted in a rapid increase in emission ratio of Ven/Turq over a 3-min time frame. In contrast, the emission ratio of Ven/Turq in cells expressing mTurquoise-10AA-Venus did not change with Fsk treatment during this same time frame (Fig. 4). This indicates that the detected change in FRET signals in cells expressing AKAR4.1 biosensor is specific, reflecting the changes in intracellular PKA activity in the cardiomyocytes in response to Fsk. The range of emission ratios determined for individual cardiomyocytes expressing AKAR4.1 from two independent experiments that included a total of 12 cells was 1.13 to 1.647.

Monitoring FRET-based biosensor probe activities using IVM. We next applied our 2PE ratiometric method to measure the effect of glucagon on PKA activity in cells in the intact mouse liver, using IVM to monitor the changes in the AKAR4.1 signal. Treatment of fasted mice with glucagon has been shown to rapidly stimulate both cAMP and PKA in the cells of the liver in situ (18). The AKAR4.1 biosensor was introduced into mice by tail vein injection of an adenoviral vector, resulting in extensive expression in the mouse liver after 7 days. Prior to imaging by IVM the mice were fasted for 3 h. The left lateral lobe of the liver was then externalized and imaged by IVM through a glass-bottom plate using methods previously described (30). Using the same microscope settings described above, three-dimensional image volumes (10 planes spanning 10 μm) were collected over time prior to and following intraperitoneal injection of glucagon (200 μg/kg). Each volume was then summed, and background-corrected mean Ven/Turq ratios were determined for ROIs in the cytosol or nuclei for several cells in the field (Fig. 5). The results demonstrate a rapid and significant increase in the emission in the Venus channel with a concomitant decrease of the cyan fluorescence within 1.5 min of glucagon administration, indicating a rapid and sustained activation of PKA. As with the results obtained with HEK293 cells, glucagon-induced activation of PKA was restricted to the cytosol of hepatocytes in vivo because of the slow translocation of the catalytic subunit of PKA into the nucleus (Fig. 5). The responses of individual hepatocytes to glucagon stimulation were variable, as is expected for the heterogeneous cellular components of the liver. The range of emission ratios determined for individual hepatocytes expressing AKAR4.1 from three independent experiments that included a total of 32 cells was 1.14 to 1.827. Taken together, the results demonstrate a simple and robust method using single-wavelength 2PE to monitor the activity of a FRET-based biosensor in an intact animal by IVM.

DISCUSSION

The imaging of fluorescent probes in cells in the tissues of intact organisms using IVM is being increasingly applied in many fields of biology and has become a method of choice for a wide variety of applications. 2PE is used in most applications of IVM, owing to its relative immunity to the effects of light scatter in tissue. However, the use of 2PE to monitor FRET-

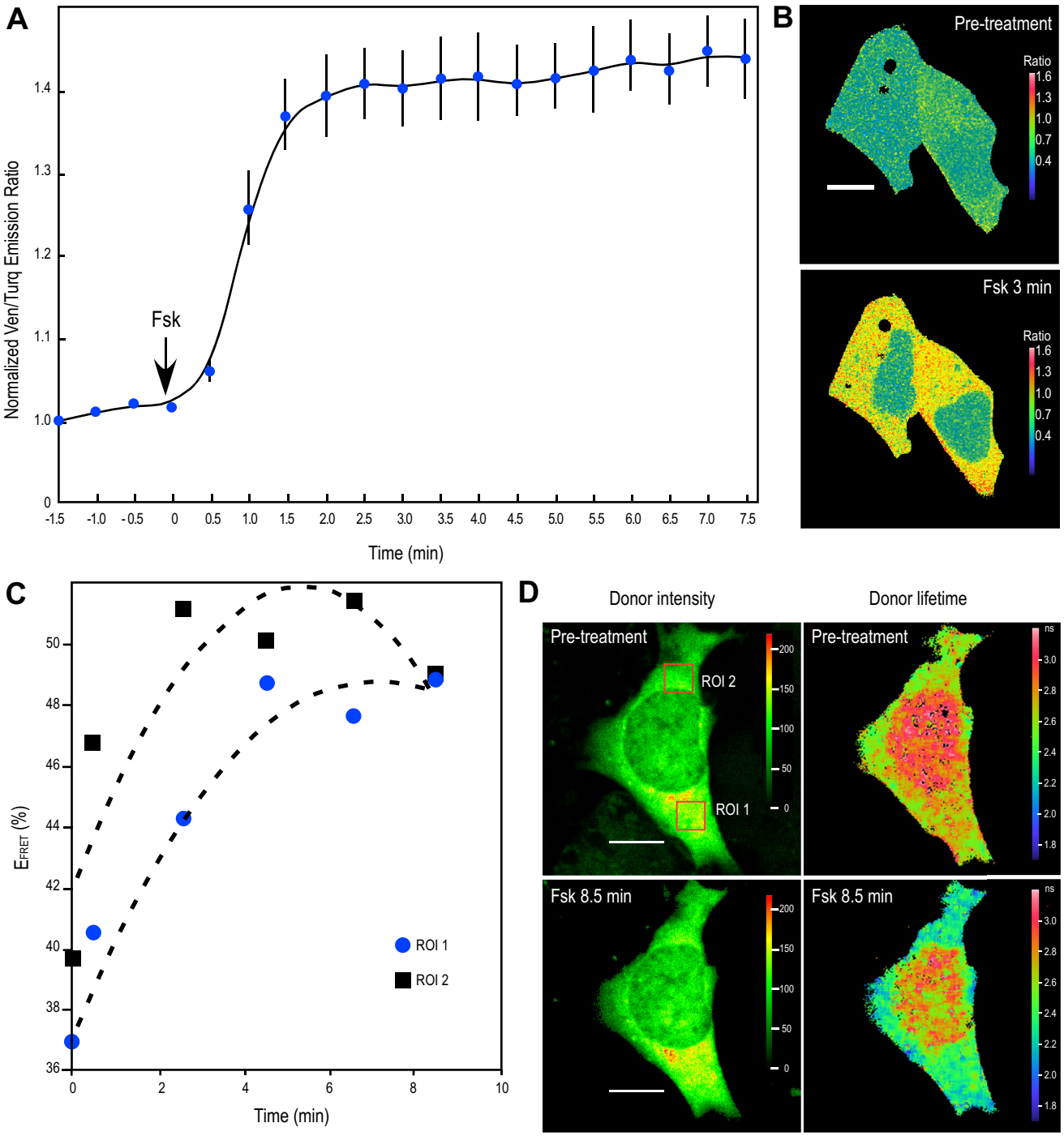

Fig. 3. *A*: ratiometric measurements of the response of the AKAR4.1 probe to forskolin (Fsk) treatment in living cells. HEK293 cells expressing the AKAR4.1 reporter were illuminated at 810 nm, and the emission signals were simultaneously monitored in the donor (454–494 nm) and acceptor (520–580 nm) channels. The Ven/Turq ratio was determined as described in RESULTS. *B*: FRET ratio images of cells prior to and 3 min after Fsk treatment. *C*: the change in AKAR4.1 FRET efficiency (E_{FRET}) upon Fsk treatment was determined by lifetime measurements using *Eq. 4* for the regions of interest (ROI) indicated in *D*. *D*: intensity images and lifetime maps for a cell prior to and 8.5 min after Fsk treatment (scale bar, 10 μm).

based biosensor probe activities in intact animals has remained challenging because of poorly characterized 2PE probe characteristics, the requirements for using two separate excitation wavelengths, and the potential need to collect multiple images at each time point. Here, we developed a practical 2PE approach to monitor biosensor activity in living animals from a single, two-channel image collected in vivo.

The systematic analysis of the 2PE characteristics of potential FP pairs for IVM revealed that mTurquoise and mVenus are well suited for FRET-based biosensor probes for 2PE IVM. There are distinct advantages of this FP pairing for IVM biosensor probes compared with the other FPs tested. First, the cyan FPs are optimally excited near the power maximum of the titanium-sapphire lasers typically

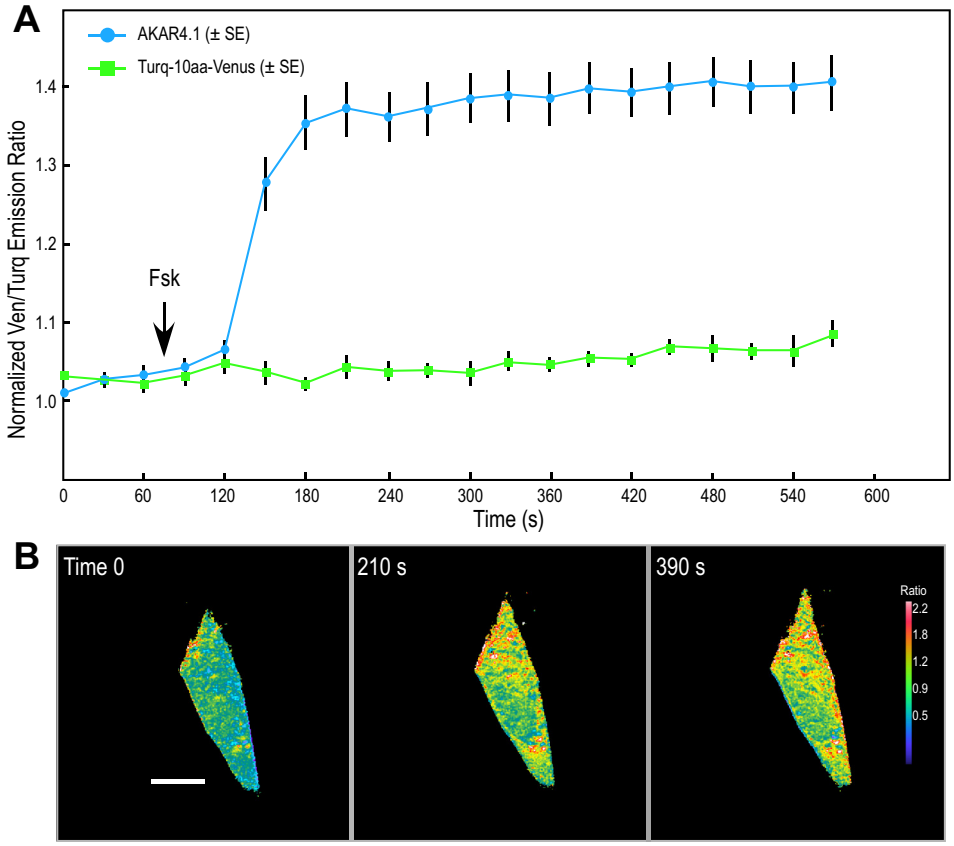

Fig. 4. *A*: ratiometric measurements of the response of the AKAR4.1 probe to forskolin (Fsk) in isolated primary mouse fetal cardiomyocytes. Freshly isolated primary cardiomyocytes were transfected with either the plasmid encoding AKAR4.1 or the mTurquoise-10AA-Venus FRET standard. There was a rapid increase in the Ven/Turq ratio for the cells expressing AKAR4.1, but not the FRET standard over a 3-min time frame. The results for AKAR4.1 are from the 9 individual cells (± SE). *B*: ratio images of a single cardiomyocyte at the indicated time points (scale bar, 10 μm).

used for 2PE microscopy. While the usefulness of the earlier variants of the cyan FPs was limited by poor brightness and photostability, and unfavorable photoswitching behavior, the newer versions of these probes, including mTurquoise, have largely overcome these problems (7, 8, 17, 32). Second, mVenus is an efficient FRET acceptor for mTurquoise, but it is minimally excited between 800 nm and 820 nm. This reduces the fluorescence cross talk caused by the direct excitation of mVenus at the wavelengths used to excite mTurquoise. Finally, many existing FRET-based biosensor probes were developed with earlier variants of the cyan and yellow FPs, so most imaging systems are already designed for the detection of these probes.

Here, the FRET standard approach was used to substantiate mTurquoise and mVenus for 2PE ratiometric measurements. Furthermore, this approach enabled the development of a simple and robust correction method to obtain accurate determinations of E_{FRET} with high sensitivity from two-channel images of the biosensor probes expressed in cells of intact animals. It is important to point out that the cross talk corrections we identified are specific to our system and must be determined for each microscope. Here, we provided a straightforward method for this evaluation. We demonstrated that 2PE measurements for cells expressing each of the FRET standards produced the expected FRET efficiency (E_{FRET}), as validated by FLIM and verified by acceptor photobleaching. The sensitivity of the approach was demonstrated in the direct comparison of the FRET standards with linker lengths of 5AA and 10AA. Measurements using the 2PE approach clearly distinguished an 11% decrease in E_{FRET} for the standard with the longer linker—a difference that was verified by the FLIM. This demonstrates that the approach can be used to obtain accurate measurements of E_{FRET} with high sensitivity from the linked probes expressed in living cells.

The approach was validated for biosensor probes using AKAR4.1 to detect changes in the activity of PKA. The single 2PE wavelength ratiometric measurement detected rapid and specific changes in cytoplasmic PKA activity in cultured HEK293 cells and primary cardiomyocytes in response to treatment with forskolin and in hepatocytes in the liver of living mice upon stimulation with glucagon. These results demonstrate that this simple approach, using a standard multiphoton microscope system, can enable the noninvasive detection of FRET-based biosensor activities in intact mice at high spatiotemporal resolution. A similar 2PE ratiometric approach was used earlier to detect calpain or caspase-3 protease activity in vivo (1, 12, 33). The linkers separating the FPs in the sensing units of these biosensors contain the substrate for a specific protease, with the cleavage of the linker reporting protease activity that is typically associated with the onset of cell death. The resulting "on-off" FRET signal can be a powerful tool in studies of responses to therapeutic strategies (12). In contrast, the conformational biosensors such as AKAR detect the dynamic response to cellular signaling events, with ratiometric measurements of biosensor activity reporting the changing spatiotemporal landscape of cell signaling (5, 19, 37, 39, 40, 42).

It is important to recognize that measurements collected at greater depth in vivo will have a higher detection threshold because of signal attenuation at depth (10). Furthermore, there

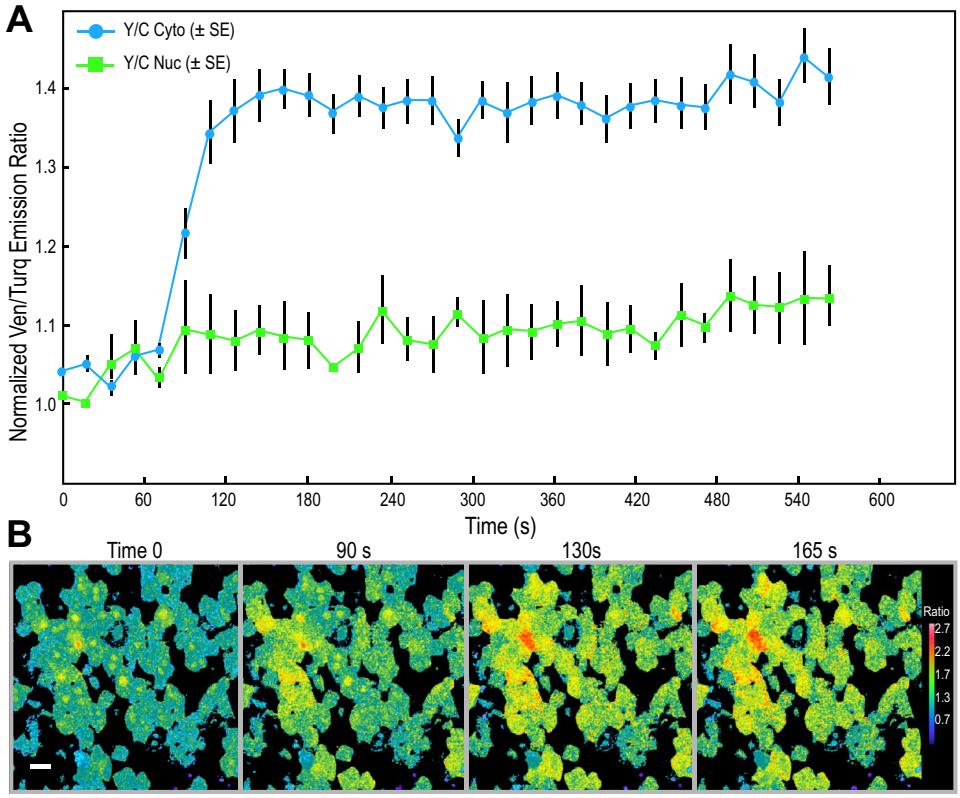

Fig. 5. *A*: intravital microscopy (IVM) measurements of the response of the AKAR4.1 probe to glucagon in hepatocytes in the intact mouse liver. The AKAR4.1 biosensor was introduced into mice by tail vein injection of an adenoviral vector encoding AKAR4.1, resulting in extensive expression in the liver 7 days later. Mice were fasted for 3 h prior to imaging by IVM, and three-dimensional image volumes (10 planes spanning 10 μm) were collected over time prior to and following intraperitoneal injection of glucagon (200 μg/kg). Each volume was then summed, and background-corrected Ven/Turq ratios were determined for ROIs in the cytosol or nuclei for several cells in the field. The results for AKAR4.1 are from the 10 individual cells (± SE). *B*: ratio images from a single image plane in mouse liver at the indicated time points (scale bar, 10 μm).

are wavelength-dependent differences in scattering that could introduce depth-dependent effects on ratiometric measurements collected in biological tissues. While we found no evidence of a significant effect of depth on our measurements, the studies of Radbruch et al. (26) did indicate minor effects of depth on ratiometric FRET measurements. Therefore, studies collected over a large range of depths should be evaluated for systematic effects of depth on ratiometric measures. In addition, differences in the susceptibility of the donor and acceptor to photobleaching could affect the measured ratios. The effects of photobleaching can be minimized by careful control of illumination levels (26).

Some of the problems associated with 2PE ratiometric imaging can be mitigated by using the FRET-FLIM approach. FLIM measurements are made only in the donor channel, and they quantify the change in donor lifetime that occurs as the result of FRET. Since the measurements are made in the time domain, they are unaffected by variations in probe concentration or by changes in the excitation intensity (4). The FRET-FLIM approach was used for intravital measurements of neuronal calcium fluctuations in response to chronic inflammation in the central nervous system of living mice (27, 26). This approach, however, requires the collection of enough photons to accurately assign lifetimes, which can be limiting for deep-tissue imaging, and may require long acquisition times that would limit dynamic measurements.

The approach described here could be improved in two respects. First, we recognize that the use of an optical parametric oscillator (OPO) for tuneable excitation from ~1,100 nm to 1,300 nm would greatly expand the useful FPs available for 2PE FRET studies (41). For example, the use of green and red FPs for intravital FRET measurements reduces light scatter at depth, and there are improved FPs for this application (15, 38). The continued development of red and near infrared FPs will greatly expand this approach. OPO, however, adds to an already complex and expensive microscope system (36). Second, because of equipment limitations, we collected the fluorescence emissions using descanned spectral detectors. Since scattered fluorescence emissions can be better captured using nondescanned detectors, more efficient collection of images from tissue at depth could be accomplished using nondescanned detectors, equipped with optical filters optimized for the emission spectra of mTurquoise and mVenus. Third, our approach was predicated on the need to rapidly collect images using a single excitation wavelength. Multiphoton microscope systems are increasingly deployed with multiple lasers, or single lasers providing multiple emission lines. Such systems would support rapid collection of fluorescence stimulated at different excitation wavelengths and would not be limited to ratiometric measurements of linked probes.

Here, we have demonstrated a straightforward and sensitive 2PE method for monitoring FRET-based biosensor activities at high spatiotemporal resolution in cells in living animals. Although demonstrated for the AKAR4.1 probe, we expect that the mTurquoise/mVenus pair could be applied to a variety of different FRET-based biosensors. Thus, the approach described here could be used to translate many of the kinds of studies currently conducted in cultured cells to the in situ context of the living animal, supporting powerful and exciting new studies of cellular biochemistry and signaling in vivo.

ACKNOWLEDGMENTS

We thank Dr. Malgorzata Kamocka and Seth Winfree for assistance in microscopy, and Paula Cranfill (Florida State University) for the plasmids encoding the fluorescent proteins. Microscopy studies were conducted at the Indiana Center for Biological Microscopy.

GRANTS

This research was supported by the National Institutes of Health O'Brien Center for Advanced Renal Microscopic Analysis (NIH-NIDDK P30DK079312).

DISCLOSURES

No conflicts of interest, financial or otherwise, are declared by the author(s).

AUTHOR CONTRIBUTIONS

W.T., M.R., J.R., X.X., C.Q., T.H., M.W.D., and R.N.D. performed experiments; W.T. analyzed data; W.T., K.W.D., and R.N.D. interpreted results of experiments; W.T., M.R., J.R., X.X., C.Q., T.H., K.W.D., and R.N.D. edited and revised manuscript; W.T., M.R., J.R., X.X., C.Q., T.H., M.W.D., K.W.D., and R.N.D. approved final version of manuscript; K.W.D. and R.N.D. conception and design of research; K.W.D. and R.N.D. drafted manuscript; R.N.D. prepared figures.

REFERENCES

1. **Breart B, Lemaitre F, Celli S, Bousso P.** Two-photon imaging of intratumoral $CD8^+$ T cell cytotoxic activity during adoptive T cell therapy in mice. *J Clin Invest* 118: 1390–1397, 2008.
2. **Broussard JA, Rappaz B, Webb DJ, Brown CM.** Fluorescence resonance energy transfer microscopy as demonstrated by measuring the activation of the serine/threonine kinase Akt. *Nat Protoc* 8: 265–281, 2013.
3. **Chen TS, Zeng SQ, Luo QM, Zhang ZH, Zhou W.** High-order photobleaching of green fluorescent protein inside live cells in two-photon excitation microscopy. *Biochem Biophys Res Commun* 291: 1272–1275, 2002.
4. **Day RN.** Measuring protein interactions using Forster resonance energy transfer and fluorescence lifetime imaging microscopy. *Methods* 66: 200–207, 2014.
5. **DiPilato LM, Zhang J.** Fluorescent protein-based biosensors: resolving spatiotemporal dynamics of signaling. *Curr Opin Chem Biol* 14: 37–42, 2010.
6. **Drobizhev M, Makarov NS, Tillo SE, Hughes TE, Rebane A.** Two-photon absorption properties of fluorescent proteins. *Nat Methods* 8: 393–399, 2011.
7. **Goedhart J, van Weeren L, Hink MA, Vischer NO, Jalink K, Gadella TW Jr.** Bright cyan fluorescent protein variants identified by fluorescence lifetime screening. *Nat Methods* 7: 137–139, 2010.
8. **Goedhart J, von Stetten D, Noirclerc-Savoye M, Lelimousin M, Joosen L, Hink MA, van Weeren L, Gadella TW Jr, Royant A.** Structure-guided evolution of cyan fluorescent proteins towards a quantum yield of 93%. *Nat Commun* 3: 751, 2012.
9. **Griesbeck O, Baird GS, Campbell RE, Zacharias DA, Tsien RY.** Reducing the environmental sensitivity of yellow fluorescent protein. Mechanism and applications. *J Biol Chem* 276: 29188–29194, 2001.
10. **Heim N, Garaschuk O, Friedrich MW, Mank M, Milos RI, Kovalchuk Y, Konnerth A, Griesbeck O.** Improved calcium imaging in transgenic mice expressing a troponin C-based biosensor. *Nat Methods* 4: 127–129, 2007.
11. **Helmchen F, Denk W.** Deep tissue two-photon microscopy. *Nat Methods* 2: 932–940, 2005.
12. **Janssen A, Beerling E, Medema R, van Rheenen J.** Intravital FRET imaging of tumor cell viability and mitosis during chemotherapy. *PLos One* 8: e64029, 2013.
13. **Koushik SV, Chen H, Thaler C, Puhl HL 3rd, Vogel SS.** Cerulean, Venus, and VenusY67C FRET reference standards. *Biophys J* 91: L99–L101, 2006.
14. **Kremers GJ, Hazelwood KL, Murphy CS, Davidson MW, Piston DW.** Photoconversion in orange and red fluorescent proteins. *Nat Methods* 6: 355–358, 2009.
15. **Lam AJ, St-Pierre F, Gong Y, Marshall JD, Cranfill PJ, Baird MA, McKeown MR, Wiedenmann J, Davidson MW, Schnitzer MJ, Tsien RY, Lin MZ.** Improving FRET dynamic range with bright green and red fluorescent proteins. *Nat Methods* 9: 1005–1012, 2012.

15a. **Lindquist R, Niesner R.** *Intravital FRET: comprehending life at single-molecule level*. Focus on "A practical method for monitoring FRET-based biosensors in living animals using two-photon microscopy." *Am J Physiol Cell Physiol* (October 14, 2015). doi:10.1152/ajpcell.00286.2015.

16. **Luo J, Deng ZL, Luo X, Tang N, Song WX, Chen J, Sharff KA, Luu HH, Haydon RC, Kinzler KW, Vogelstein B, He TC.** A protocol for rapid generation of recombinant adenoviruses using the AdEasy system. *Nat Protoc* 2: 1236–1247, 2007.
17. **Markwardt ML, Kremers GJ, Kraft CA, Ray K, Cranfill PJ, Wilson KA, Day RN, Wachter RM, Davidson MW, Rizzo MA.** An improved cerulean fluorescent protein with enhanced brightness and reduced reversible photoswitching. *PLos One* 6: e17896, 2011.
18. **Miller RA, Chu Q, Xie J, Foretz M, Viollet B, Birnbaum MJ.** Biguanides suppress hepatic glucagon signalling by decreasing production of cyclic AMP. *Nature* 494: 256–260, 2013.
19. **Miyawaki A.** Development of probes for cellular functions using fluorescent proteins and fluorescence resonance energy transfer. *Annu Rev Biochem* 80: 357–373, 2011.
20. **Nagai T, Ibata K, Park ES, Kubota M, Mikoshiba K, Miyawaki A.** A variant of yellow fluorescent protein with fast and efficient maturation for cell-biological applications. *Nat Biotechnol* 20: 87–90, 2002.
21. **Ni Q, Titov DV, Zhang J.** Analyzing protein kinase dynamics in living cells with FRET reporters. *Methods* 40: 279–286, 2006.
22. **Park YC, Burkitt V, Villa AR, Tong L, Wu H.** Structural basis for self-association and receptor recognition of human TRAF2. *Nature* 398: 533–538, 1999.
23. **Patterson GH, Piston DW.** Photobleaching in two-photon excitation microscopy. *Biophys J* 78: 2159–2162, 2000.
24. **Periasamy A, Day RN.** *Molecular Imaging: FRET Microscopy and Spectroscopy*. New York: Oxford Univ. Press, 2005, p. 312.
25. **Pittet MJ, Weissleder R.** Intravital imaging. *Cell* 147: 983–991, 2011.
26. **Radbruch H, Bremer D, Mothes R, Gunther R, Rinnenthal JL, Pohlan J, Ulbricht C, Hauser AE, Niesner R.** Intravital FRET: probing cellular and tissue function in vivo. *Int J Mol Sci* 16: 11713–11727, 2015.
27. **Rinnenthal JL, Bornchen C, Radbruch H, Andresen V, Mossakowski A, Siffrin V, Seelemann T, Spiecker H, Moll I, Herz J, Hauser AE, Zipp F, Behne MJ, Niesner R.** Parallelized TCSPC for dynamic intravital fluorescence lifetime imaging: quantifying neuronal dysfunction in neuroinflammation. *PLos One* 8: e60100, 2013.
28. **Rizzo MA, Springer GH, Granada B, Piston DW.** An improved cyan fluorescent protein variant useful for FRET. *Nat Biotechnol* 22: 445–449, 2004.
29. **Rizzo MA, Springer G, Segawa K, Zipfel WR, Piston DW.** Optimization of pairings and detection conditions for measurement of FRET between cyan and yellow fluorescent proteins. *Microsc Microanal* 12: 238–254, 2006.
30. **Ryan JC, Dunn KW, Decker BS.** Effects of chronic kidney disease on liver transport: quantitative intravital microscopy of fluorescein transport in the rat liver. *Am J Physiol Regul Integr Comp Physiol* 307: R1488–R1492, 2014.
31. **Shaner NC, Steinbach PA, Tsien RY.** A guide to choosing fluorescent proteins. *Nat Methods* 2: 905–909, 2005.
32. **Shaner NC, Lin MZ, McKeown MR, Steinbach PA, Hazelwood KL, Davidson MW, Tsien RY.** Improving the photostability of bright monomeric orange and red fluorescent proteins. *Nat Methods* 5: 545–551, 2008.
33. **Stockholm D, Bartoli M, Sillon G, Bourg N, Davoust J, Richard I.** Imaging calpain protease activity by multiphoton FRET in living mice. *J Mol Biol* 346: 215–222, 2005.
34. **Thaler C, Koushik SV, Blank PS, Vogel SS.** Quantitative multiphoton spectral imaging and its use for measuring resonance energy transfer. *Biophys J* 89: 2736–2749, 2005.
35. **Tillo SE, Hughes TE, Makarov NS, Rebane A, Drobizhev M.** A new approach to dual-color two-photon microscopy with fluorescent proteins. *BMC Biotechnol* 10: 6, 2010.
36. **Timpson P, McGhee EJ, Anderson KI.** Imaging molecular dynamics in vivo–from cell biology to animal models. *J Cell Sci* 124: 2877–2890, 2011.
37. **VanEngelenburg SB, Palmer AE.** Fluorescent biosensors of protein function. *Curr Opin Chem Biol* 12: 60–65, 2008.
38. **Yasuda R, Harvey CD, Zhong H, Sobczyk A, van Aelst L, Svoboda K.** Supersensitive Ras activation in dendrites and spines revealed by

two-photon fluorescence lifetime imaging. *Nat Neurosci* 9: 283–291, 2006.
39. **Zhang J, Ma Y, Taylor SS, Tsien RY.** Genetically encoded reporters of protein kinase A activity reveal impact of substrate tethering. *Proc Natl Acad Sci USA* 98: 14997–15002, 2001.
40. **Zhang J, Campbell RE, Ting AY, Tsien RY.** Creating new fluorescent probes for cell biology. *Nat Rev Mol Cell Biol* 3: 906–918, 2002.
41. **Zhang W, Parsons M, McConnell G.** Flexible and stable optical parametric oscillator based laser system for coherent anti-Stokes Raman scattering microscopy. *Microsc Res Tech* 73: 650–656, 2010.
42. **Zhou X, Herbst-Robinson KJ, Zhang J.** Visualizing dynamic activities of signaling enzymes using genetically encodable FRET-based biosensors from designs to applications. *Methods Enzymol* 504: 317–340, 2012.
43. **Zipfel WR, Williams RM, Webb WW.** Nonlinear magic: multiphoton microscopy in the biosciences. *Nat Biotechnol* 21: 1369–1377, 2003.